Article

Toward Planar Iodine 2D Crystal Materials

Xinyue Zhang and Qingsong Huang*

Read Online

ACCESS | Metrics & More | Article Recommendations | Supporting Information

ABSTRACT: Usually, the octet rule determines whether an elemental 2D material can only be set by one of the elements in groups IIIA−VA, whose outmost electrons can form hybridized orbits from an s-wave and a p-wave. The hybridized orbits can accommodate all of the outermost electrons and form robust σ bonds. As for the elements in VIA−VIIA, the outermost electrons seem too abundant to be accommodated in hybridized orbits. Here, we show a spd^2 hybridization rule, accommodating all of the outermost electrons of halogen elements. Each atom can be connected to a contiguous atom by a robust σ bond and carries one dangling unpaired electron, implying that the formation of a π bond is possible. One iodine atomic layer can be robustly locked by

the σ bond, forming an iodiene sheet by spd^2 hybridized orbits. With application of compression strain, the π bond forms, and further compression drives the band inversion successively at the valence band and the conduction band. The appearance of Dirac points (arc or hoop) suggests that the transformation of a normal semimetal into a Dirac semimetal occurs.
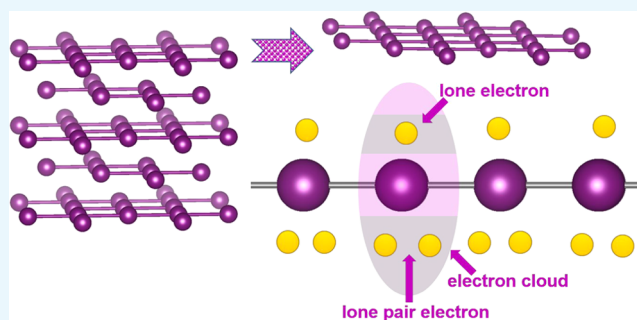
1. INTRODUCTION

As for 2D materials,[1] e.g., graphene, the unpaired dangling electrons on the exact contiguous atoms can form weak π bonds and finally develop into a structure with a linear energy dispersion for survival of massless Dirac Fermions.[2,3] In particular, main VA group elements, such as phosphorous,[4] arsenic,[5] antimony,[6] and bismuth,[7] form elemental 2D materials mainly with σ bonds, arising from the hybridization of p-waves with a small number of s-waves.[8] The Dirac points, as a nontrivial points, arise from the appearance of band inversion,[9−12] instead of just formation of π bonds.[8] The π bonds just provide a possibility of forming a linear energy dispersion to accommodate massless Dirac Fermions.[13,14] By far, five outmost electrons are the maximum limitation for the sp^2 hybridization, and three electrons, the minimum one; therefore, groups IIIA−VA are generally regarded as the limitation of scope for forming elemental 2D materials by s-wave and p-wave—hybridized orbits.[15]

As for the VIA and VIIA elements, however, formation of elemental 2D materials remains challenging. Since the outmost electron number is more than six and formation of 2D materials needs at least three covalent bonds and six electrons, violation of the octet rule is inevitable. Empty d orbits are necessary to be hybridized with s and p orbits to form s−p−d hybridized orbits, accommodating the redundant electrons. In addition, the covalent σ bonds between elements should be strong enough to sustain the frame of the 2D configurations.

Here, we present 2D materials arising from elements of group VIIA, constructing σ bonds by spd^2 hybridized orbits. Although the s−p−d hybridization can survive in some specific

molecules,[16,17] it has never been observed in infinite 2D periodic crystals before.

So far, some literature studies have reported the 3D iodine molecule (I_2) crystalline stacked by 2D molecular layers, transforming into an in-plane covalently-connected atomic layer with interplanar van der Waals connection by a pressure-induced process.[18−22] The crystalline I_2 molecule is composed of atomically thin layers stacked by coplanar zigzag networks, where there are both in-plane and interplanar van der Waals forces. The I_2 molecule dissociates into atoms, induced by high pressures, triggering the in-plane atoms to become connected with covalent bonding, whereas the interplane atoms interact by van der Waals force. The pressure-induced covalent bond will be available because of s−p−d hybridized orbits.[18]

According to the experiment references,[18] iodiene does exist under high pressures. Herewith, we try to construct iodiene in a stable state, obtaining a tetragonal 2D configuration by DFT geometrical optimization. As for the tetragonal 2D configuration crystal material, the atoms are connected by spd^2 hybridized σ bonds, while the π key in high-symmetry points is difficult to form because of the long bond length (LBL), despite the dangling unpaired electron being available for each atom.[23−25] Formation of Dirac points depends on band
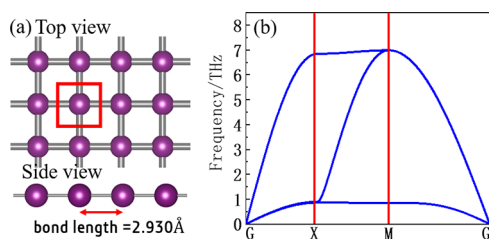
21235
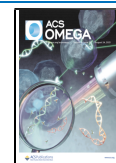
inversion,[26] bond length reductions to form π bonds,[27] or perturbation of Anderson potential barriers.[28] The phonon spectrum calculation shows that iodine can form stable two-dimensional materials (Figure 1). In the absence of strain, the

Figure 1. Structure and phonon spectra of iodiene. (a) Structural model illustrating a single layer with a planar configuration and a geometric unit, which is derived from a 3D iodiene structure under high pressures.[29] The unit cell of iodiene has been marked as a red rectangle. (b) Phonon spectrum: no virtual frequency is available, implying the planar 2D configuration is stable.

LBL is too far to form the π key. When strain is applied, the LBL becomes smaller than before, and the π key can come into being gradually. After that, further increasing strain makes Dirac points available, arising from band inversion.

2. RESULTS AND DISCUSSION

2.1. Structure and Stability. As is well known, the iodine molecular crystal can be compressed under 20.6 GPa into an atomic crystal, stacked up by the 2D atomic layer iodiene,[29] where atoms connect to each other according to the tetragonal planar configuration by in-plane covalent bonds. Even though the atomic crystal is available, the iodine crystal will gradually develop from an orthorhombic to a body-centered-cubic structure,[29−31] thus activating evolution by high pressure. Since the 3D materials are composed of 2D iodiene, they interact between contiguous layers by the van der Waals force. When any layer is exfoliated from the body, the isolated layer can become free-standing. To this end, a DFT model is built up to simulate the optimized structure, demonstrating that a tetragonal iodiene configuration can exist in real space (Figure 1a, top view). The unit cell has been labeled with the red frame (Figure 1a, inset), demonstrating that the bond length is around 2.930 Å and the bond angle is 90° (Figure 1a, side view). There are no imaginary frequency in the phonon spectrum, illustrating that planar iodiene is stable. In addition, Young's modulus and Poisson's ratio of iodiene are 50 GPa and 0.38, respectively, where a binding energy of 0.843 eV/atom has been provided for mechanical stability.

2D iodiene has been realized by developing crystalline iodine molecules into atomic ones under a high pressure, e.g., 21 GPa.[29] When the tetragonal planar 2D configuration is available, it should be very stable, even if the pressure increases successively. However, the intrinsic properties change when the strain reaches a critical point. In addition, a buckling spatial configuration can be considered (Figure S3a) to be unstable, deduced from the negative phonon spectrum of the acoustic branch (Figure S3b). Moreover, the puckered spatial configuration seems impossible (Figure S1) because puckered iodiene always develops into a quasi-planar structure after geometric optimization. However, the planar tetragonal structure is robust and stable, if a specific bond length is set within the van der Waals diameter[32] (Figure S2).

2.2. Effect of Strain on the Band Structure. Usually, the band gap can be tuned by biaxial stress.[33] Since the crystalline lattice in Figure 1a has been observed in experiments, it can survive and is stable in the real space and can be selected as the starting point to be further compressed. Meanwhile, the valence bands of iodiene run across the Fermi surface, so the band gap here refers to the minimum energy difference between the HOMO and the LUMO, instead of the width of the forbidden zone based on the Fermi level. Upon applying biaxial compressive strain to 2D iodiene in real space (the bond length is 2.930 Å), it seems that a pushing force is exerted between the CB and VB in the BZ to make them close. Thus, the compression strain can induce a reduction of the band gap (Figure 2a−d). Once the compression strain reaches
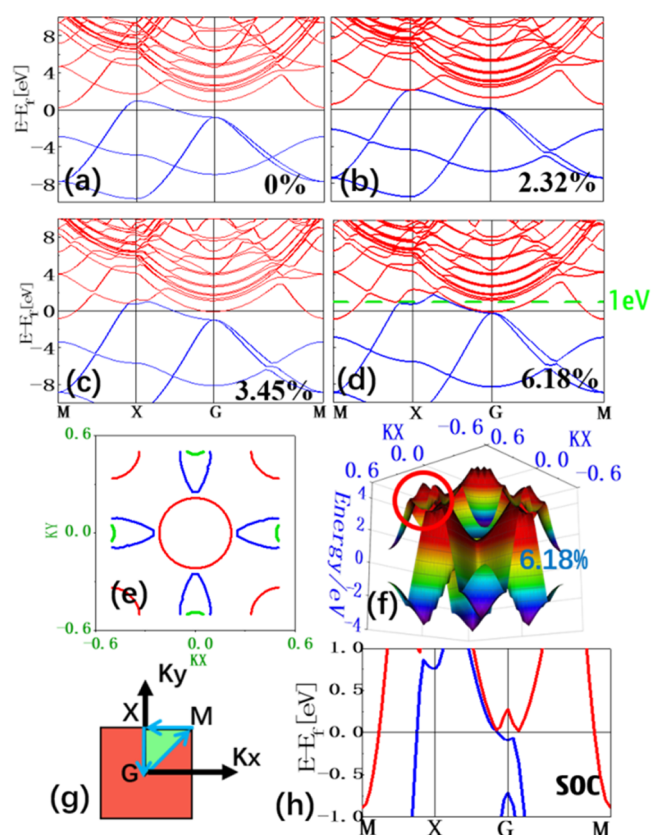

Figure 2. Band structure of iodiene under biaxial strain: (a) 0% or without strain, (b) 2.32% compressive strain, (c) 3.45% compressive strain, (d) 6.18% compressive strain, and (e) cross section of the 3D band structure along 1 eV according to (d) and (f). (f) Conduction and valence bands are assembled in 3D, showcasing the 3D band inversion at X with the red circle emphasizing the assembly points. (g) Orientation of the integral path in the momentum space of the BZ. (h) Inversion bands at γ points with SOC when the compression strain is 6.18%, which is mentioned in (d).

2.32%, the direct band gap at the X point in the Brillouin zone (BZ) approaches zero (Figure 2b), implying that the formation of a π bond is possible. Further compression to a strain of 3.45% can induce band inversion, creating Dirac points, one of the topologically nontrivial points available (Figure 2c). The 2D iodiene can transfer from a wide band gap to a Dirac semimetal[34,35] or a topological semimetal.[36] When the strain increases to 6.18%, the band inversion becomes even stronger than before near the high-symmetry X point (Figure 2d). The Dirac points or topological nontrivial points, ca. 1 eV away
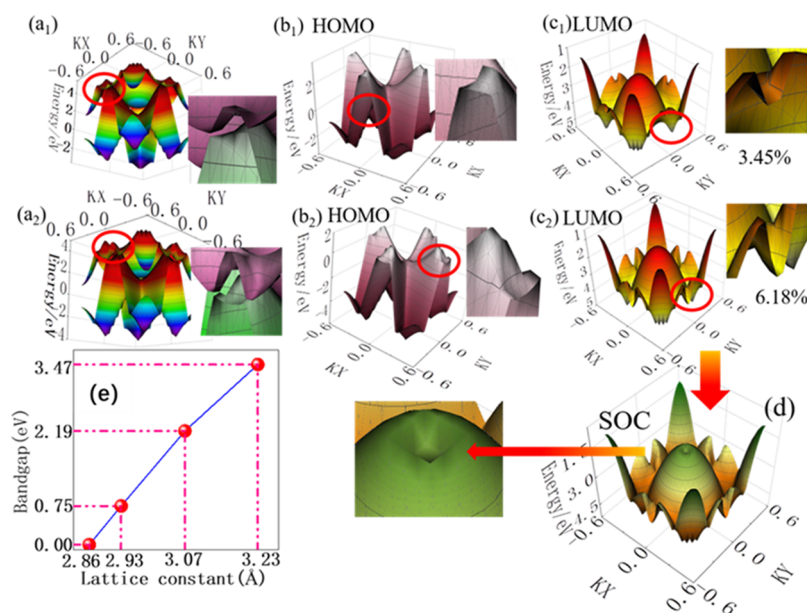
Figure 3. Iodiene 3D band structure and its constituent parts, including HOMO, LUMO, and related band inversion (red circle) under biaxial strain: (a_1–c_1) 3.45% biaxial stress and (a_2–c_2) 6.18% biaxial stress. The red circle points out the inversion part, whose enlarged view is shown in the inset. If the SOC effect is applied to iodiene with biaxial strain, a band inversion configuration at the γ point to LUMO (c_2) can be observed (d and green inset), which is inverted by 180° to stand on its back in comparison to its normal structure. (e) Relationship between lattice constants and band gaps.
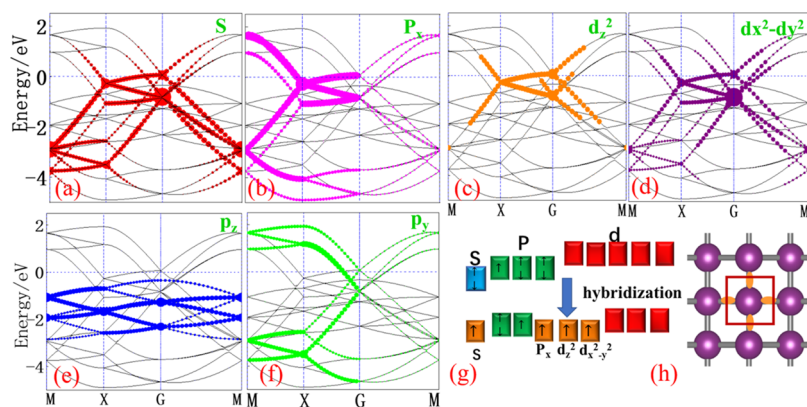
Figure 4. Hybridized orbit of iodiene. (a–f) Band structure and occupied orbital energy level for iodiene, suggesting that the hybridized orbital is formed by contribution from four spd^2 orbitals: p_x, s, d_{zz} and d_{xx-yy}. (g) Schematics of orbital levels and orbit hybridization. The hybridized orbital received a contribution from the d orbit in the same shell, accommodating the electrons from the s, p_x orbits. (h) Schematic diagram of the hybridized orbit in iodiene, and the yellow bonds represent the 4 σ bonds, arising from hybridized orbits.

from the Fermi level, can be linked into arcs (Figure 2e), implying the Dirac semimetal[35,36] or the topological semimetal state. The Dirac plane at 1 eV has been applied to check the arc, where the red arcs represent its cross section with the conduction bands, and the blue curves represent the valence bands. However, the green arcs are composed of Dirac points, suggesting the conductance by Dirac Fermions has become stronger than that with only Dirac points.

The inverted band structures of the 3D structures are shown in Figures 2f and 3. The 3D band structures with biaxial stress are shown in Figure 2f, where the compression strain at 6.18% has been demonstrated. However, the 3D band structure in Figure 2f illustrates the Dirac points lying in contact with each other (inset: red circle), where the Dirac semimetal can be viewed. All of the high-symmetry points can be found in Figure 2g. Interestingly, when the compressive strain reaches 6.18%, the CB and VB come into contact at γ points (Figure 2d) and

the Fermi level, implying that the 2D iodiene can be grown into an epitaxial film on some specific substrates because most of the 2D materials can be subjected to biaxial compressive strain by substrates.[37−40] In addition, if considering the spin−orbit coupling (SOC) effect, the contact point will develop into an inversion band (Figure 2h), suggesting that the Dirac points emerge as an intrinsic property of the epitaxial film.

The 3D band structures illustrate the band inversion structure in detail (Figure 3). Since applying the compressive strain in real space is just like exerting a compressive force between the CB and VB in the BZ, increasing compressive strain can make HOMO and LUMO close, even to zero. After that, further strain can make the band inversion in both the VB and CB occur at the contacting point in the BZ. When the compression strain reaches 3.45%, the band inversion occurs both in HOMO and LUMO simultaneously at the four high-symmetry points X in the BZ (Figure 3a_1 and inset), where the

inset illustrates the enlarged red-circled part to check the inversion band at the high-symmetry point X. As for the valence band inversion, the 3D HOMO (Figure 3b$_1$ and inset) shows that the bands have inverted to a concave structure, implying that the inversion happens around X points.

The LUMO structure has been turned by 180° to stand on its back (Figure 3c$_1$, and inset); the circled area and inset mark the inversion structure. On increasing the strain to 6.18% (Figure 3a$_2$, and inset), the band inversion becomes even stronger than that with the strain of 3.45% both in HOMO (Figure 3b$_2$ and inset) and LUMO (Figure 3c$_2$ and inset) around X points. In addition, a new contact happens in the γ point (Figure 3c$_2$ and inset). Moreover, if SOC is applied, a band inversion can be obtained at the γ point (Figure 3d and inset). Except for the SOC, further strain can induce the band inversion around γ points (Figure S3). As can be seen from Figure 3e, when the lattice constant of iodiene is between 2.86 and 3.23 Å, the size of the band gap is linearly related to the lattice constant.

2.3. Orbital Hybridization. The band hybridization is shown in Figure 4, where the spd^2 hybridized orbitals can be observed from the band structure and occupied orbital energy level (Figure 4a–f), mimicking each other at a similar energy level. Four covalent σ bonds can form the frame plane of iodiene (FPI), sustaining the stability. However, the unpaired electron tends to form the π bond, depending on the reduction of the bond length to 2.86 Å. When the bond length is within van der Waals diameters (4.30 Å),[32] a covalent bond will be available. Usually, when the bond length is less than 3.0 Å, the band inversion should be possible, inducing the Dirac Fermion survival.

The hybrid orbits come from almost equal energy levels (Figure S5) over s, p, d at the same period and the same shell in the iodine atom. The s-wave and p-wave have the most important contribution and d has much weaker contribution (Figure S6) to the spd^2 hybridized orbit, forming the covalent connection with σ bonds to sustain the system.

The hybridization energy level diagram (Figure 4g) illustrates the hybridized orbits (Figure 4g, yellow), the primitive p-wave orbits (Figure 4g, green), and empty orbits (Figure 5g, red). The spatial configuration is shown in Figure

4h, where the unpaired single electron and lone pair electron orbits are mounted on the opposite side of the FPI plane (Figure 5). The unpaired single electrons are active and become dangling bonds, implying that a potential π bond can be formed if the bond length is shortened enough. Provided the bond length becomes much shorter than before, the weak antilocalization has an opportunity to activate the electrical conductance, implying that the band gap approaches zero. If the compression strain is strong enough to trigger the interaction between two contiguous lone electron pairs, the lone pair electron orbit can be activated, making iodiene buckled and behave like that in BP.[41] However, here, only the planar configuration is available, suggesting that a lone electron pair has no effective interaction with its adjacent one, instead, the unpaired single electron or dangling bonds have.

Electronic local functions (ELFs)[42] are presented to demonstrate the binding energy between the atoms (Figure 5). From blue to ultrared, the corresponding value means the covalent bond becomes stronger gradually (Figure 5a, legend). Here, the ELF value is around 0.2−0.6 (Figure 5a, top view), implying a weak bond level in comparison to graphene.[43] Moreover, a side view (Figure 5a) and the 3D images (Figure 5b) confirm that the atoms in iodiene are connected by covalent bonds with a bond length of 3.234 Å, much less than the van der Waals diameter, suggesting that the covalent bond is strong enough to support the 2D configuration (Figure 5a, bottom side view). The ellipse shape, instead of circle, represents that the deformed shape arises from the strong covalent bonds and the difference between covalent bonds and dangling bonds (Figure 5a,b, bottom side view). As shown in Figure 5c, according to a specific spd^2 hybridization rule, the dangling unpaired electron is permitted to form the π key and even develop into Dirac points if the bond length is reduced effectively. The interaction between atoms includes three parts. (1) σ−σ bonds, (2) π−π bonds, and (3) lone pair−lone pair interaction. Here, only the σ−σ bond works. The dangling unpaired electron should become the π−π bond if LBL is suitable. With the application of compressive strain, the π−π bond becomes activated into the linear energy dispersion relation finally. If a severe strain is applied, the lone pair−lone pair interaction might be active.

3. CONCLUSIONS

The 2D material, iodiene, really exists at extremely high pressures. Moreover, after DFT optimization, iodiene can be obtained as a Dirac Fermion material and even a topological nontrivial semimetal. Our findings have opened a new route to 2D crystals by applying a special hybridization rule, by which the same shell d-wave orbit can hybridize with the s-wave and p-wave orbits. It is also possible to prepare iodiene at atmospheric pressure by selecting a suitable substrate.[44,45]

4. CALCULATION METHODS

First-principles calculations were performed by the plane-wave code Vienna Ab initio Simulation Package (VASP).[46] The calculations were carried out within the generalized-gradient approximation (GGA) with the Perdew−Burke−Ernzerhof functional (PBE) and density-functional theory (DFT).[47] The wave functions between the cores were expanded in plane waves with a kinetic energy cutoff of 400 eV. The convergence criterion of the electron self-consistent loop was set to 10^{-8} eV, and the force convergence criterion was set to 0.01 eV/Å. The
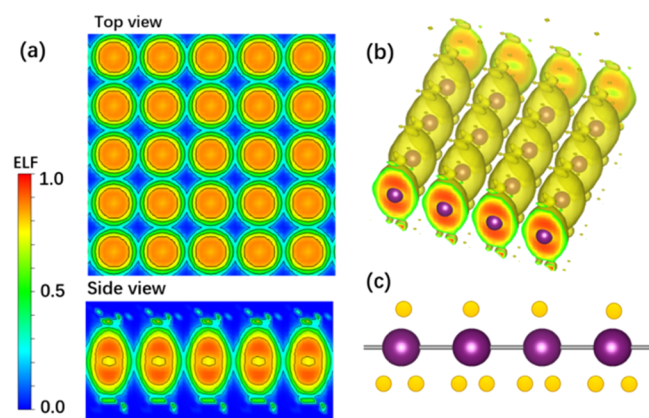
Figure 5. Electron local function (ELF) of iodiene. (a) Top view and side view of the ELF diagrams demonstrate that the bonding mode of iodiene has covalent properties. (b) Electron local function diagram, mimicking an egg (ellipsoid) since the covalent interaction between the contiguous atoms is much different from that of (c) the dangling unpaired electron and lone pair one.

K-mesh scheme is Gamma and uses 0.03 $2\pi/\text{Å}$ accuracy for *K* point sampling in the reciprocal space. The pressure was applied by setting the stress parameter in the INCAR file of VASP. To prevent the interaction of periodic structures, a 30 Å vacuum layer was used. The phonon spectrum was calculated by the DFPT algorithm with a $2 \times 2 \times 1$ supercell.[48] According to the following formula

$$E_b = E_{at} - E_{sheet} \qquad (1)$$

the binding energy of materials (E_b) is calculated,[49] where E_{at} is the energy of an isolated spin polarized atom and E_{sheet} is the energy of each atom in the two-dimensional materials.

By multiplying the lattice constants *a* and *b* by the same scaling coefficient, the biaxial strain is implemented. For the primitive cells of the *p4mmm* space group, the lattice constants *a* and *b* are equivalent and the calculation of the uniaxial strain is realized by multiplying one of the lattice constants by the corresponding scaling coefficient. This article was previously published as a preprint.[50]

ASSOCIATED CONTENT

Supporting Information

The Supporting Information is available free of charge at https://pubs.acs.org/doi/10.1021/acsomega.1c00628.

    Different configurations of iodiene; 3D band structure of iodiene; and PDOS of iodiene (PDF)

AUTHOR INFORMATION

Corresponding Author

Qingsong Huang − *School of Chemical Engineering, Sichuan University, Chengdu 610065, P. R. China;* ⓘ orcid.org/0000-0002-1104-8806; Email: qshuang@scu.edu.cn

Author

Xinyue Zhang − *School of Chemical Engineering, Sichuan University, Chengdu 610065, P. R. China*

Complete contact information is available at:
https://pubs.acs.org/10.1021/acsomega.1c00628

Author Contributions

Q.H. conceived the project and performed the main analysis of data. X.Z. performed the calculation and simulation. All authors discussed the results and wrote the paper.

Notes

The authors declare no competing financial interest.
The raw/processed data required to reproduce these findings cannot be shared at this time as the data also form part of an ongoing study.

ACKNOWLEDGMENTS

REFERENCES

(1) Mas-Ballesté, R.; Gomez-Navarro, C.; Gomez-Herrero, J.; Zamora, F. 2D materials: to graphene and beyond. *Nanoscale* **2011**, *3*, 20−30.

(2) Katsnelson, M. I. Graphene: carbon in two dimensions. *Mater. Today* **2007**, *10*, 20−27.

(3) Mannix, A. J.; Kiraly, B.; Hersam, M. C.; Guisinger, N. P. Synthesis and chemistry of elemental 2D materials. *Nat. Rev. Chem.* **2017**, *1*, No. 0014.

(4) Guo, Z. N.; Zhang, H.; Lu, S. B.; Wang, Z. T.; Tang, S. Y.; Shao, J. D.; Sun, Z. B.; Xie, H. H.; Wang, H. Y.; Yu, X. F.; Chu, P. K. From Black Phosphorus to Phosphorene: Basic Solvent Exfoliation, Evolution of Raman Scattering, and Applications to Ultrafast Photonics. *Adv. Funct. Mater.* **2015**, *25*, 6996−7002.

(5) Kamal, C.; Ezawa, M. Arsenene: Two-dimensional buckled and puckered honeycomb arsenic systems. *Phys. Rev. B* **2015**, *91*, No. 085423.

(6) Ares, P.; Palacios, J. J.; Abellan, G.; Gomez-Herrero, J.; Zamora, F. Recent Progress on Antimonene: A New Bidimensional Material. *Adv. Mater.* **2018**, *30*, No. 1703771.

(7) Lu, L.; Liang, Z. M.; Wu, L. M.; Chen, Y. X.; Song, Y. F.; Dhanabalan, S. C.; Ponraj, J. S.; Dong, B. Q.; Xiang, Y. J.; Xing, F.; Fan, D. Y.; Zhang, H. Few-layer Bismuthene: Sonochemical Exfoliation, Nonlinear Optics and Applications for Ultrafast Photonics with Enhanced Stability. *Laser Photonics Rev.* **2018**, *12*, No. 1700221.

(8) Pumera, M.; Sofer, Z. 2D Monoelemental Arsenene, Antimonene, and Bismuthene: Beyond Black Phosphorus. *Adv. Mater.* **2017**, *29*, No. 1605299.

(9) Zhang, T.; Mu, Y.; Zhao, J. Z.; Hu, C. E.; Chen, X. R.; Zhou, X. L. Quantum anomalous/valley Hall effect and tunable quantum state in hydrogenated arsenene decorated with a transition metal. *Phys. Chem. Chem. Phys.* **2018**, *20*, 12138−12148.

(10) Liu, M. Y.; Chen, Q. Y.; Cao, C.; He, Y. Topologically nontrivial phase and tunable Rashba effect in half-oxidized bismuthene. *Phys. Chem. Chem. Phys.* **2019**, *21*, 2899−2909.

(11) Chuang, F. C.; Hsu, C. H.; Chen, C. Y.; Huang, Z. Q.; Ozolins, V.; Lin, H.; Bansil, A. Tunable topological electronic structures in Sb(111) bilayers: A first-principles study. *Appl. Phys. Lett.* **2013**, *102*, No. 022424.

(12) Cheung, C. H.; Fuh, H. R.; Hsu, M. C.; Lin, Y. C.; Chang, C. R. Spin Orbit Coupling Gap and Indirect Gap in Strain-Tuned Topological Insulator-Antimonene. *Nanoscale Res. Lett.* **2016**, *11*, No. 459.

(13) Novoselov, K. S.; Geim, A. K.; Morozov, S. V.; Jiang, D.; Katsnelson, M. I.; Grigorieva, I. V.; Dubonos, S. V.; Firsov, A. A. Two-dimensional gas of massless Dirac fermions in graphene. *Nature* **2005**, *438*, 197−200.

(14) Park, C. H.; Yang, L.; Son, Y. W.; Cohen, M. L.; Louie, S. G. New generation of massless Dirac fermions in graphene under external periodic potentials. *Phys. Rev. Lett.* **2008**, *101*, No. 126804.

(15) Gupta, A.; Sakthivel, T.; Seal, S. Recent development in 2D materials beyond graphene. *Prog. Mater. Sci.* **2015**, *73*, 44−126.

(16) Tam, D. W.; Berlijn, T.; Maier, T. A. Stabilization of s-wave superconductivity through arsenic p-orbital hybridization in electron-doped BaFe₂As₂. *Phys. Rev. B* **2018**, *98*, No. 024507.

(17) Vega, A.; Dorantesdavila, J.; Balbas, L. C.; Pastor, G. M. Calculated Sp-Electron and Spd-Hybridization Effects on the Magnetic-Properties of Small Fe(N) Clusters. *Phys. Rev. B* **1993**, *47*, 4742−4746.

(18) Takemura, K.; Sato, K.; Fujihisa, H.; Onoda, M. Incommensurately modulated phase of iodine under high pressure. *Ferroelectrics* **2004**, *305*, 103−106.

(19) Shimomura, C.; Takemura, K.; Fujii, Y.; Minomura, S.; Mori, M.; Noda, Y.; Yamada, Y. Structure-Analysis of High-Pressure Metallic State of Iodine. *Phys. Rev. B* **1978**, *18*, 715−719.

(20) Riggleman, B. M.; Drickamer, H. G. Approach to metallic state as obtained from optical and electrical measurements. *J. Chem. Phys.* **1963**, *38*, 2721−2724.

(21) Lynch, R. W.; Drickame, H. G. Effect of pressure on lattice parameters of iodine stannic iodide and p-di-iodobenzene. *J. Chem. Phys.* **1966**, *45*, 1020−1026.

(22) Fujii, Y.; Hase, K.; Hamaya, N.; Ohishi, Y.; Onodera, A.; Shimomura, O.; Takemura, K. Pressure-induced face-centered-cubic phase of monatomic metallic iodine. *Phys. Rev. Lett.* **1987**, *58*, 796−799.

(23) Zhang, S.; Yan, Z.; Li, Y.; Chen, Z.; Zeng, H. Atomically thin arsenene and antimonene: semimetal-semiconductor and indirect-direct band-gap transitions. *Angew. Chem., Int. Ed.* **2015**, *54*, 3112−3115.

(24) Sanchez-Palencia, L.; Clement, D.; Lugan, P.; Bouyer, P.; Aspect, A. Disorder-induced trapping versus Anderson localization in Bose-Einstein condensates expanding in disordered potentials. *New J. Phys.* **2008**, *10*, No. 045019.

(25) Modugno, G. Anderson localization in Bose-Einstein condensates. *Rep. Prog. Phys.* **2010**, *73*, No. 102401.

(26) Yang, B.-J.; Nagaosa, N. Classification of stable three-dimensional Dirac semimetals with nontrivial topology. *Nat. Commun.* **2014**, *5*, No. 4898.

(27) Saeidi, P.; Nourbakhsh, Z. The investigation of topological phase of $Gd_{1-x}Y_xAuPb$ (x = 0, 0.25, 0.5, 0.75, 1) alloys under hydrostatic pressure. *J. Magn. Magn. Mater.* **2018**, *451*, 681−687.

(28) Bieniek, M.; Wozniak, T.; Potasz, P. Stability of topological properties of bismuth (111) bilayer. *J. Phys.: Condens. Matter* **2017**, *29*, No. 155501.

(29) Fujii, Y.; Hase, K.; Hamaya, N.; Ohishi, Y.; Onodera, A.; Shimomura, O.; Takemura, K. Pressure-induced face-centered-cubic phase of monatomic metallic iodine. *Phys. Rev. Lett.* **1987**, *58*, 796−799.

(30) Natsume, Y.; Suzuki, T. Calculation of the electronic band-structure for the hole metal state of iodine in high-pressure phase. *Solid State Commun.* **1982**, *44*, 1105−1107.

(31) Takemura, K.; Minomura, S.; Shimomura, O.; Fujii, Y. Observation of molecular dissociation of iodine at high-pressure by x-ray-diffraction. *Phys. Rev. Lett.* **1980**, *45*, 1881−1884.

(32) Jones, R. G.; Kadodwala, M. Bromine adsorption on Cu(111). *Surf. Sci.* **1997**, *370*, L219−L225.

(33) Peng, X. H.; Wei, Q.; Copple, A. Strain-engineered direct-indirect band gap transition and its mechanism in two-dimensional phosphorene. *Phys. Rev. B* **2014**, *90*, No. 085402.

(34) Mendoza-Sánchez, B.; Gogotsi, Y. Synthesis of two-dimensional materials for capacitive energy storage. *Adv. Mater.* **2016**, *28*, 6104−6135.

(35) Kim, J.; Baik, S. S.; Ryu, S. H.; Sohn, Y.; Park, S.; Park, B.-G.; Denlinger, J.; Yi, Y.; Choi, H. J.; Kim, K. S. Observation of tunable band gap and anisotropic Dirac semimetal state in black phosphorus. *Science* **2015**, *349*, 723−726.

(36) Hasan, M. Z.; Xu, S.-Y.; Belopolski, I.; Huang, S.-M. Discovery of Weyl Fermion Semimetals and Topological Fermi Arc States. *Annu. Rev. Condens. Matter Phys.* **2017**, *8*, 289−309.

(37) Dai, Z.; Liu, L.; Zhang, Z. Strain engineering of 2d materials: issues and opportunities at the interface. *Adv. Mater.* **2019**, *31*, No. 1805417.

(38) Jeganathan, K.; Shimizu, M. Importance of growth temperature on achieving lattice-matched and strained InAlN/GaN heterostructure by plasma-assisted molecular beam epitaxy. *AIP Adv.* **2014**, *4*, No. 097113.

(39) Ni, Z. H.; Chen, W.; Fan, X. F.; Kuo, J. L.; Yu, T.; Wee, A. T. S.; Shen, Z. X. Raman spectroscopy of epitaxial graphene on a SiC substrate. *Phys. Rev. B* **2008**, *77*, No. 115416.

(40) Sahatiya, P.; Solomon Jones, S.; Thanga Gomathi, P.; Badhulika, S. Flexible substrate based 2D ZnO (n)/graphene (p) rectifying junction as enhanced broadband photodetector using strain modulation. *2D Mater.* **2017**, *4*, No. 025053.

(41) Guo, Z.; Zhang, H.; Lu, S.; Wang, Z.; Tang, S.; Shao, J.; Sun, Z.; Xie, H.; Wang, H.; Yu, X.-F.; Chu, P. K. From black phosphorus to phosphorene: basic solvent exfoliation, evolution of raman scattering, and applications to ultrafast photonics. *Adv. Funct. Mater.* **2015**, *25*, 6996−7002.

(42) Terriberry, T. B.; Cox, D. F.; Bowman, D. A. A tool for the interactive 3D visualization of electronic structure in molecules and solids. *Comput. Chem.* **2002**, *26*, 313−319.

(43) Qin, Z.; Qin, G.; Hu, M. Origin of anisotropic negative Poisson's ratio in graphene. *Nanoscale* **2018**, *10*, 10365−10370.

(44) Ahn, G. H.; Amani, M.; Rasool, H.; Lien, D.-H.; Mastandrea, J. P.; Ager, J. W., III; Dubey, M.; Chrzan, D. C.; Minor, A. M.; Javey, A. Strain-engineered growth of two-dimensional materials. *Nat. Commun.* **2017**, *8*, No. 608.

(45) Chang, C.-Y.; Lin, H.-T.; Lai, M.-S.; Yu, C.-L.; Wu, C.-R.; Chou, H.-C.; Lin, S.-Y.; Chen, C.; Shih, M.-H. Large-area and strain-reduced two-dimensional molybdenum disulfide monolayer emitters on a three-dimensional substrate. *ACS Appl. Mater. Interfaces* **2019**, *11*, 26243−26249.

(46) Kresse, G.; Furthmuller, J. Efficient iterative schemes for ab initio total-energy calculations using a plane-wave basis set. *Phys. Rev. B* **1996**, *54*, 11169−11186.

(47) Perdew, J. P.; Burke, K.; Ernzerhof, M. Generalized gradient approximation made simple. *Phys. Rev. Lett.* **1996**, *77*, 3865−3868.

(48) Baroni, S.; de Gironcoli, S.; Dal Corso, A.; Giannozzi, P. Phonons and related crystal properties from density-functional perturbation theory. *Rev. Mod. Phys.* **2001**, *73*, 515−562.

(49) Tang, H.; Ismail-Beigi, S. Novel precursors for boron nanotubes: the competition of two-center and three-center bonding in boron sheets. *Phys. Rev. Lett.* **2007**, *99*, No. 115501.

(50) Zhang, X. Y.; Huang, Q. S. Towards Planar Iodine 2D Crystal Materials. 2019, arXiv:1909.07604. arXiv.org e-Print archive. https://arxiv.org/abs/1909.07604 (accessed Sept 17, 2019).